RSC Advances

PAPER

View Article Online
View Journal | View Issue

Cite this: *RSC Adv.*, 2021, **11**, 20200

Improved efficiency and air stability of two-dimensional p-i-n inverted perovskite solar cells by Cs doping†

Tzu-Chien Hsieh,[ae] Chung-Yueh Shih,[ae] Yu-Chiang Chao,[*b] I-Chun Cheng*[cdf] and Jian-Zhang Chen[*aef]

Two-dimensional perovskite solar cells (2-D PSCs) have attracted much research attention in recent years because they are more stable in a regular environment than three-dimensional (3-D) ones are. In this study, we doped Cs into 2D perovskite ($BA_2(MA)_2Pb_3I_{10}$) films as the absorbing layers of the 2-D p-i-n inverted PSCs to investigate the influence of the Cs doping concentration on the properties of the 2-D perovskite films and the fabricated solar cells. Cs doping clearly improves the power conversion efficiency (PCE) and air stability of the PSCs. Doping perovskite with 10% Cs (the best doping concentration in this study) can increase the PSC efficiency from 7.98% to 10.11%. Scanning electron microscopy indicates the improved surface quality and crystallinity by Cs doping. However, excess Cs doping degrades the PCE of the PSCs. Furthermore, 10% Cs doped PSCs show air stability superior to that of undoped ones in unpackaged humidity environments. After exposure to 55% relative humidity (RH) in 19 °C air for 300 h, the PCE of the PSC decreased by only 39%, in contrast to 84% for the undoped PSC.

Received 1st April 2021
Accepted 30th May 2021

DOI: 10.1039/d1ra02574k

rsc.li/rsc-advances

1. Introduction

Organic–inorganic hybrid perovskite solar cells (PSCs) have attracted much research attention recently because of their low cost and high efficiency.[1–8] In 2009, three dimensional (3D) methyl ammonium lead halide ($MAPbI_3$) was used to develop the first PSC, and it was based on a structure similar to a dye-sensitized solar cell.[6] This material exhibited excellent visible light absorption, high electron and hole mobilities, good defect tolerance, low surface recombination, and a suitable bandgap.[4,9–27] A PSC with a record power conversion efficiency (PCE) of 25.5% has been reported.[28] However, it contains Pb[29] and has poor air stability as it degrades rapidly in moisture and oxygen.[30] These factors have limited its commercial applications. Therefore, reducing toxicity while enhancing the air stability are critical to realized practical applications of PSCs. In this light, studies need to focus on the PSC packaging technology. However, some studies found that the degradation rate is very high even if the cell is encapsulated.[19,31]

Traditional 3D PSCs degrade in air and under humid condition, and they suffer problems such as ion migration and thermal instability; these issues lead to their poor long-term stability in air.[32] Therefore, a quasi-two-dimensional Ruddlesden–Popper perovskite device was developed and it has shown better stability in regular environments.[28,33–36] A Ruddlesden–Popper perovskite is denoted as $R_2A_{n-1}M_nX_{3n+1}$ with an octahedral structure, where R is an organic spacer cation (usually butylammonium (BA^+) or phenylethylammonium (PEA^+)), A is a small organic cation (usually $CH_3NH_3^+$(MA^+) or $HC(NH_2)_2^+$(FA^+)); M is a metal cation (lead ion (Pb^{2+}), copper ion (Cu^{2+}), or tin ion (Sn^{2+})); X is a halogenated anion (usually chloride ion (Cl^-), bromide ion (Br^-) or iodide ion (I^-)), and n is the number of structural layers; different stoichiometries perform differently.[28] Because a two-dimensional (2D) perovskite structure has a different number of layers, it has more freedom and adjustability from a chemistry viewpoint. Organic spacer cations can improve the structural stability and prevent the intrusion of moisture and the erosion of the inorganic layer.[37] The improved structural stability is attributed to the strong van der Waals interaction between the blocked organic cation and the [PbI 6]-unit.[38] Therefore, this 2D perovskite should have better moisture resistance and be suitable as a light absorber.[34,39–41] This also affects the transfer of charge between the inorganic plates, resulting in poor photovoltaic

[a]*Graduate Institute of Applied Mechanics, National Taiwan University, Taipei City 10617, Taiwan. E-mail: jchen@ntu.edu.tw*

[b]*Department of Physics, National Taiwan Normal University, Taipei City 11677, Taiwan. E-mail: ycchao@ntnu.edu.tw*

[c]*Graduate Institute of Photonics and Optoelectronics, National Taiwan University, Taipei City 10617, Taiwan. E-mail: iccheng@ntu.edu.tw*

[d]*Department of Electrical Engineering, National Taiwan University, Taipei City 10617, Taiwan*

[e]*Advanced Research Center for Green Materials Science and Technology, National Taiwan University, Taipei City 10617, Taiwan*

[f]*Innovative Photonics Advanced Research Center (i-PARC), National Taiwan University, Taipei City 10617, Taiwan*

† Electronic supplementary information (ESI) available. See DOI: 10.1039/d1ra02574k

performance.[34,38,39] The poor PCE of 2D PSC is due to the lower absorption coefficient, poorer charge transport, and large exciton binding energy.[39] The quasi-two-dimensional Ruddlesden–Popper perovskite device $(BA)_2MA_3Pb_4I_{13}$ produced using a hot casting method exhibited a PCE of 12.52%. This method can change the crystal orientation from the in-plane direction to the out-of-plane direction to form an effective charge transport layer. Therefore, this device exhibits better photovoltaic performance and moisture resistance than the 3D PSC.[41] Many methods can be used to control the crystallographic orientation and to improve the characteristics of solar cells. Different additives can be added to the precursor solution to adjust the perovskite crystallization,[42–51] for example, ammonium thiocyanate (NH_4SCN),[52,53] methyl ammonium chloride (MACl),[54] and doped metal cations.[55] Overall, adding different substances and doping metals is considered the easiest and most convenient method.

In this study, we doped Cs into 2D $(BA)_2(MA)_3Pb_3I_{10}$ ($n = 3$) perovskite to grow 2D layered perovskite crystals through a one-step spin coating method. Then, this Cs-doped 2D perovskite was used as the absorption layer of p-i-n inverted planar PSCs. To the best of our knowledge, ours is the first study of Cs-doped 2D $(BA)_2(MA)_3Pb_3I_{10}$ ($n = 3$) p-i-n inverted planar PSCs. Through the doping of Cs cations, a $(BA)_2(MA)_3Pb_3I_{10}$ perovskite film with good crystallinity $(BA)_2(MA)_3Pb_3I_{10}$ was achieved on the FTO/NiO substrate. The influence of Cs doping on the photovoltaic (PV) performance was evaluated through X-ray diffraction (XRD), scanning electron microscope (SEM), ultraviolet-visible (UV-vis) spectroscopy, water contact angle measurement, external quantum efficiency (EQE), and conductivity analysis. The solar cell structure is FTO/NiO/$(BA)_2(MA)_3Pb_3I_{10}$ ($n = 3$)/PC_{61} BM/methionine (BCP)/Ag. 10% Cs doping improved the PCE to 10.11% from 7.98%. Further, compared with 2D devices without Cs doping, it showed great air stability.

2. Experimental section

2.1 PSC fabrication

Fig. 1 shows the flowchart of PSC fabrication process. And Fig. S20† shows actual sample images of fabricated perovskite solar cells. FTO glass substrate (TEC7, ~8 Ω sq^{-1}) was cleaned sequentially in deionized water, acetone, isopropanol and UV-ozone cleaner (Jelight 42) for 15 min. The distance between the UV source and the sample was ~5 mm. Then, 0.5 M nickel acetate (99.998%, trace metals, Sigma-Aldrich) and ethanolamine (99.5%, Sigma-Aldrich) in ethanol (99%, anhydrous alcohol), stirred overnight at 60 °C, were used as the NiO precursor solution. The NiO precursor solution was spin-coated on the FTO substrate at a speed of 6000 rpm for 40 s, and then calcined at 325 °C on the hotplate for 10 min. Next, the sample was immediately placed in a nitrogen-filled glove box, and the perovskite film was deposited on the NiO film through a one-step method. The perovskite solution comprised butylamine hydroiodide (BAI, 99.5%, Lumtec), CH_3NH_3I (MAI, 98.0%, Dyesol), CsI (99.999%, metals basis, Alfa Aesar) and PbI_2 (99.999%, metals basis, Alfa Aesar) (molar ratio of $2:3-3x:3x:4$) in mixed solvents of *N*,*N*-dimethylformamide (DMF, 99.8%, Sigma-Aldrich) with concentration of 1.2 M, where x indicates the Cs doping (*i.e.* $x = 0.05$, 0.1, 0.15, and 0.2 corresponds to 5%, 10%, 15%, and 20%, respectively). The perovskite films were also prepared with 10% Cs doping but with different constituent chemical molar concentrations of 1.0 M, 1.2 M and 1.4 M. The perovskite solution was stirred at 60 °C for one day. The perovskite absorbent layer was deposited by spin coating the solution at 5000 rpm for 45 s. The thickness of the perovskite absorber was ~400 nm. Immediately after deposition, the perovskite film was annealed at 100 °C for 15 min. $PC_{61}BM$ (99.5%, nano-C) doped with DMOAP (Sigma-Aldrich, 42% methanol solution) was deposited on top of the perovskite layer. Next, 1 ml of $PC_{61}BM$ was doped with 2 μl of DMOAP and spin-coated on the perovskite film at a speed of 2000 rpm for 30 s. Then, bathocuproine (BCP, Alfa Aesar, 0.5 mg ml^{-1} in 2-propanol) was spin-coated on the $PC_{61}BM$ film at 6000 rpm for 20 s. These two layers are referred as the ETL.[56] Finally, an electron beam evaporator was used to evaporate silver as the top electrode; an 85 nm thick Ag layer with an area of 0.09 cm^2 (0.3 cm × 0.3 cm) was deposited on each cell as a cathode.

2.2 Characterization

SEM (JOEL, JSM-7800Prime) was used to examine morphology of the perovskite. The transmittance and reflectance spectra were measured using a UV-vis-NIR spectrophotometer (JASCO, V-670). The water contact angle was measured using a contact angle goniometer (Sindatek, model 100SB). The *J*–*V* curve of the PSC was measured using an electrometer (Agilent, B2902A) under the irradiation of simulated AM1.5 light (ABET, Sun 2000 Solar Simulator). The crystallinity was inspected by GIXRD (Bruker, D8DISCOVER SSS). EQE of a perovskite film was measured using a quantum efficiency measuring instrument

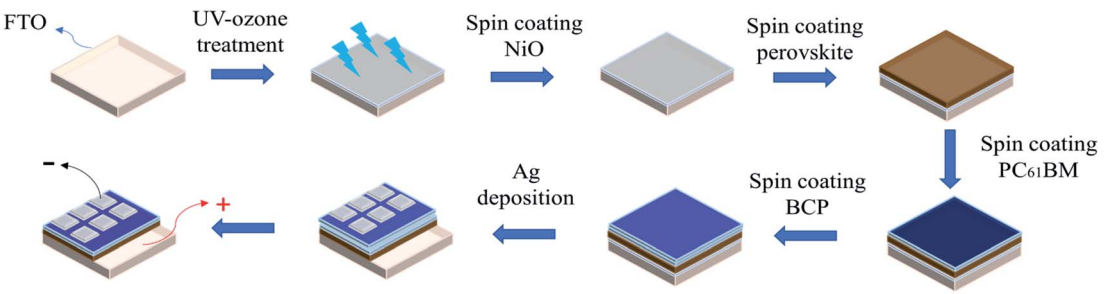

Fig. 1 Experimental flowchart.

(Enlitech, QE-R3011). The through-plane conductivity was measured using a digital sourcemeter (Keithley 2636A), in which the perovskite film (thickness: 400 nm) was deposited on the FTO glass; and a silver electrode layer was deposited directly by evaporation on the perovskite film with a defined area of 9 mm^2 and thickness of 85 nm.

3. Results and discussion

3.1 GIXRD analysis

Fig. 2 shows grazing incidence X-ray diffraction (GIXRD) results of the $BA_2(MA)_2Pb_3I_{10}$ two-dimensional perovskite on the FTO substrate. The perovskite films with and without Cs cations have (111) (2θ = 14–15°) and (202) (2θ = 29–30°) diffraction peaks; however, 10% Cs doping improves the crystallinity with the full-width-at-half-maximum reduced for both (111) and (202) peaks. This not only improves the charge transport but also leads to fewer defects and reduces charge recombination.[53] Fig. S1 and S2† show GIXRD patterns of the perovskite films with various Cs doping concentrations and prepared with various constituent chemical molar concentrations. The major difference is the intensity variation of the (111) diffraction peak. As the Cs doping concentration increases, the crystallinity first increases and then decreases. Further, a Cs doping centration of 10% results in the best crystallinity. By contrast, the crystallinity increases monotonically as the constituent chemical molar concentration increases to 1.4 M. Further, the 1.2 M case shows the best PSC performance.

3.2 SEM analysis

Fig. 3 shows images of the 2D perovskite films without/with Cs doping. With 10% Cs doping, the SEM image shows some fractal pieces. Considering the GIXRD results shown in Fig. 1, these could be crystals with better crystallinity. Larger crystal grains can reduce the trap density and grain boundary density, thereby reducing non-radiative carrier recombination.[57] Fig. S3† shows top-view SEM images of perovskite doped with different Cs concentrations, and Fig. S4† shows top-view SEM images of the perovskite doped with 10% Cs but prepared with various constituent chemical molar concentration (as described later in the Experimental section). All these images show fractal pieces.

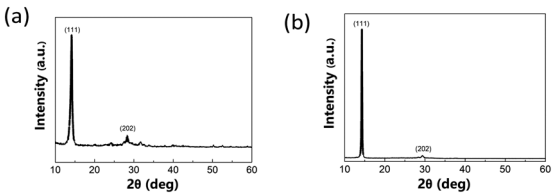

Fig. 2 GIXRD diffraction patterns of 2D perovskite film (a) without and (b) with 10% Cs doping.

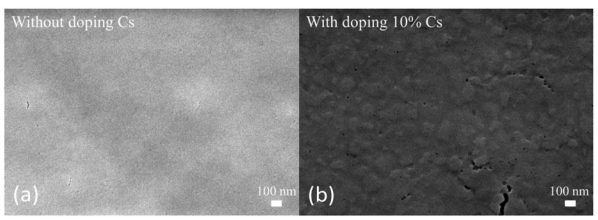

Fig. 3 SEM top view images of 2D perovskite films (a) without and (b) with 10% Cs doping.

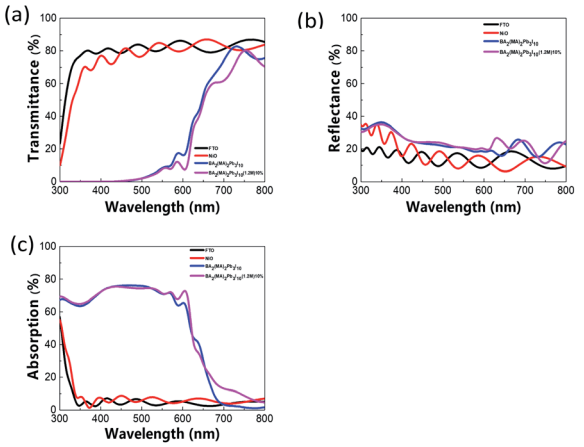

Fig. 4 UV-vis spectra of perovskite film: (a) transmittance, (b) reflectance, and (c) absorption spectra.

3.3 UV-vis analysis

Fig. 4(a)–(c) shows the transmittance (T), reflectance (R), and absorption ($1 - T - R$) spectra, respectively. After 10% Cs doping, the absorption increases slightly by 10–20% in the range between ~650 nm and ~800 nm. This may help improve the PSC performance. Fig. S5(c)† shows the spectra of the perovskite film with various Cs doping concentrations, and Fig. S6(c)† shows the spectra of films prepared with various constituent chemical molar concentrations. With various Cs

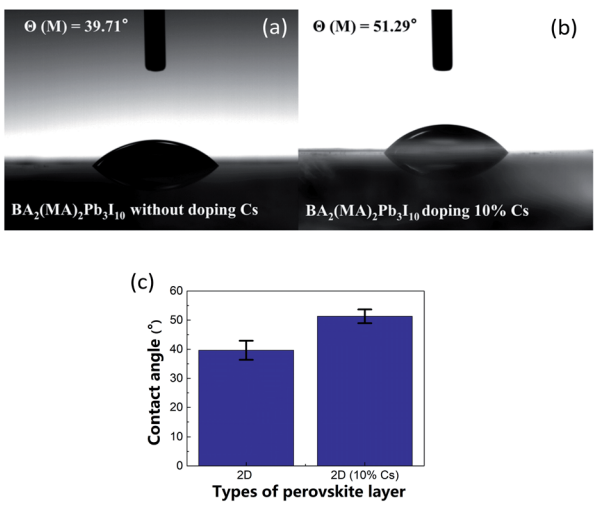

Fig. 5 Water contact angle images of 2D perovskite films: (a) without Cs doping and (b) with 10% Cs doing, and (c) water contact angle comparison with error bar.

doping concentrations, no apparent difference is seen in the absorption spectra. With regard to the constituent chemical molar concentrations, the case with 1.2 M results in better absorption between ~700 nm and ~800 nm and between ~300 nm and ~420 nm.

3.4 Water contact angle analysis

Fig. 5 shows water contact angle measurement results of the perovskite films without/with 10% Cs doping. The undoped and 10% Cs doped perovskite films show the a contact angle of 39.7° and 51.3°, respectively. The wettability difference could influence the follow-up spin-coating of the electron transport layer (ETL). Fig. S7† shows water contact angle measurement results with various Cs doping concentrations. The water contact angle first increases and then decreases as the Cs doping concentration increases. The perovskite film exhibits the highest water contact angle with 10% Cs doping. Fig. S8† shows that 10% Cs doped perovskite films prepared with various constituent chemical molar concentrations have similar water contact angles.

3.5 EQE analysis

Fig. 6 shows the EQE and corresponding integrated photocurrent curve of the inverted structure solar cell with $BA_2(MA)_2Pb_3I_{10}$ 2D perovskite as the absorbing layer. The results show that the PSC with 10% Cs doping exhibits better in EQE and corresponding integrated photocurrent. The integrated photocurrent increases from 5.544 to 12.462 mA cm^{-2} with 10% Cs doping. Fig. S9 and S10† show that the EQE and integrated photocurrent improve for all Cs doping concentrations (5%, 10%, 15%, and 20%) and for perovskite films prepared with all constituent chemical molar concentrations (1.0 M, 1.2 M, and 1.4 M for 10% Cs doping).

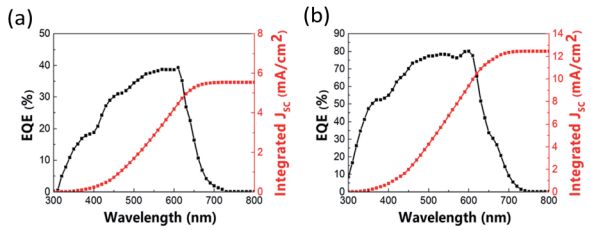

Fig. 6 EQE and corresponding integrated photocurrent curve of perovskite solar cell: (a) without Cs doping and (b) with 10% Cs doping.

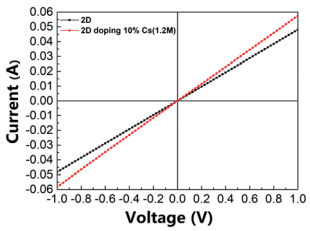

Fig. 7 Voltage–current relation of perovskite film without/with 10% Cs doping.

Table 1 Through-plane conductivity of perovskite film without/with 10% Cs doping

Perovskite film	Conductivity (mS m^{-1})
$BA_2(MA)_2Pb_3I_{10}$ without Cs doping	$2.14 \pm 9.59112 \times 10^{-3}$
$BA_2(MA)_2Pb_3I_{10}$ with 10% Cs doping	$2.56 \pm 1.64175 \times 10^{-2}$

3.6 Through-plane conductivity analysis

Fig. 7 shows the through-plane conductivity of the perovskite layer without/with 10% Cs doping; Table 1 lists the corresponding conductivity values. The conductivity increased from 2.14 to 2.56 mS m^{-1} with 10% Cs doping. Tables S1 and S2† show the detailed conductivity data with various Cs doping concentrations and for films prepared with various constituent chemical molar concentrations with 10% Cs doping. The conductivity first increased and then decreased as the Cs doping concentration increased from 0% to 20%, and it showed its maximum value with 10% Cs doping. With regard to the constituent chemical molar concentrations, a film prepared with a concentration of 1.2 M showed the best conductivity. This could be because a film prepared with a constituent chemical molar concentration of 1.2 M and with 10% Cs doping exhibits improved crystallinity with fewer defects.

3.7 PCEs upon various air exposure durations

Fig. 8 shows the relationship between the normalized PCE of the 2D PSC and the testing time for the unencapsulated PSC exposed to air (19 °C, 55% RH). This research is to investigate the environmental stability of components with and without doping 10% Cs. The long-term stability of the perovskite solar cells placed in the air was measured without any encapsulation of the element at a room temperature of 19 °C and a relative humidity of 55%. The results indicate that 10% Cs doping seemingly improved the air stability. After 300 h of exposure, the PCE retention rate was 61%, in contrast to 16% in the case of the undoped one (forward scan). Table 2 lists the PCEs of PSCs with different air exposure durations. At the same time, this also shows that proper doping of Cs can effectively enhance the PSCs' resistance to atmospheric moisture and oxygen. In other words, the results clearly indicate that Cs doping results in

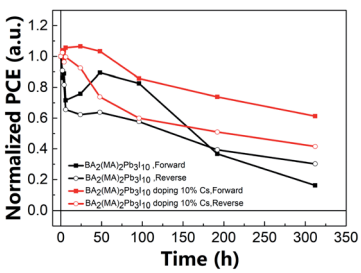

Fig. 8 Comparison of the PCEs of 2D PSCs without/without 10% Cs doping upon various air exposure durations.

Table 2 Through-plane conductivity of perovskite film without/with 10% Cs doping

	$BA_2(MA)_2Pb_3I_{10}$ without Cs doping, PCE (%)		$BA_2(MA)_2Pb_3I_{10}$ with 10% Cs doping, PCE (%)	
Time	Forward	Reverse	Forward	Reverse
0 h	6.588	6.702	6.376	8.297
2 h	5.676	6.084	6.630	8.495
4 h	5.853	5.469	6.235	7.99
6 h	4.716	4.393	6.735	8.262
24 h	4.997	4.174	6.793	7.672
48 h	5.890	4.275	6.586	6.122
96 h	5.440	3.869	5.466	4.975
192 h	2.421	2.640	4.705	4.23
312 h	1.069	2.025	3.910	3.447

improved resistance to moisture and oxygen. Tables S3, S4, Fig. S13, and S14† present more detailed data.

3.8 PV parameters statistical analysis

Fig. S15, S16, and Table S5† show statistical data of six batches of PSCs made with various Cs doping concentrations. Further, Fig. S17, S18, and Table S6† show data for films prepared with various constituent chemical molar concentrations. Four PV parameters, PCE, short circuit current density (J_{sc}), open circuit voltage (V_{oc}), and fill factor (FF) are compared. Reverse scans show better PCEs of PSCs. PV parameters deteriorate in all cases other than 10% Cs doping case. This indicates the critical role of the Cs doping concentration.[55] Fig. 9 shows *J–V* curves of the best-performing PSCs without/with 10% Cs doping. The best performing PSC with 10% Cs doping shows V_{oc} of 1.190 V, J_{sc} of 13.342 mA cm^{-2}, FF of 0.637, and PCE of 10.111%. By contrast, the best-performing PSC without Cs doping shows a similar V_{oc}, J_{sc} of 10.9 mA cm^{-2}, and PCE of only 7.984%. Further, 10% Cs doping resulted in the largest hysteresis, defined as (PCE (forward scan) − PCE (reverse scan))/PCE (forward scan), as shown in Fig. S19.† Most studies attribute hysteresis to the combination of ion migration and nonradiative recombination near the interface layer.[58] As described above, due to the increase in the hydrophobicity of the perovskite film, the increase in the conductivity of the film, the improvement in the quality of the film, the increase in crystalline grains, and the decrease in the density of defects and grain boundaries, all these factors account for the improvement of component performance, and this is also consistent with the photoelectric performance.

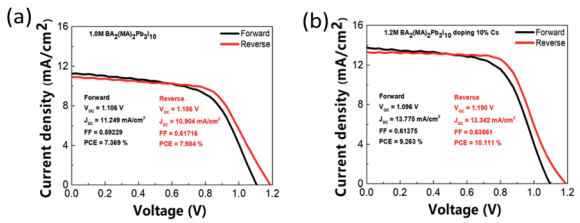

Fig. 9 *J–V* curves of best-performing PSCs (a) without and (b) with 10% Cs doping.

4. Conclusion

This study investigated the Cs-doped 2D $(BA)_2(MA)_3Pb_3I_{10}$ (n = 3) perovskite and its use as the absorbing layer of p-i-n inverted planar PSCs. The results indicated that 10% Cs doping improved the PCE of the PSC and the stability when exposed to air. The PCE of the best-performing PSC improved from 7.98% to 10.11%. After 300 h of exposure to air (19 °C, 55% RH), the PCE retention rate is 61%, in contrast to 16% in the case of the undoped PSC (forward scan). At the same time, the hysteresis of the PSC with 10% Cs doping degraded.

Author contributions

TCH conducted the experiments, perform data analyses, and write the first paper draft. CYS assisted in experiments. YCC, ICC, and JZC led the project and revised the paper.

Conflicts of interest

There are no conflicts to declare.

Acknowledgements

JZC gratefully acknowledges the funding support from "Advanced Research Center for Green Materials Science and Technology" from The Featured Area Research Center Program of the Higher Education Sprout Project by the Ministry of Education (110L9006) and the Ministry of Science and Technology in Taiwan (MOST 110-2634-F-002-043 and MOST 108-2221-E-002-088-MY3). YCC thanks the Ministry of Science and Technology of Taiwan for funding support (MOST 106-2112-M-003-016-MY3 and MOST 108-2923-M-003-001-MY3). ICC and YCC gratefully acknowledge funding support from National Taiwan University System Young Scholar Innovative Collaboration Program under grant no. NTU-IOTP-109PNTUS04. We would like to thank Ms. Yuan-Tze Lee for her assistance with the SEM operation at the Instrument Center of National Taiwan University. XRD was conducted at the Precious Instrumentation Center of National Taiwan University of Science and Technology.

References

1 J.-P. Correa-Baena, M. Saliba, T. Buonassisi, M. Grätzel, A. Abate, W. Tress and A. J. S. Hagfeldt, *Energy Environ. Sci.*, 2017, **358**, 739–744.
2 D. B. Mitzi, K. Chondroudis and C. R. Kagan, *IBM J. Res. Dev.*, 2001, **45**, 29–45.
3 D. B. Mitzi, *J. Mater. Chem.*, 2004, **14**, 2355–2365.
4 J. Burschka, N. Pellet, S.-J. Moon, R. Humphry-Baker, P. Gao, M. K. Nazeeruddin and M. Grätzel, *Nature*, 2013, **499**, 316–319.

5 H.-S. Kim, C.-R. Lee, J.-H. Im, K.-B. Lee, T. Moehl, A. Marchioro, S.-J. Moon, R. Humphry-Baker, J.-H. Yum and J. E. Moser, *Sci. Rep.*, 2012, **2**, 1–7.
6 A. Kojima, K. Teshima, Y. Shirai and T. Miyasaka, *J. Am. Chem. Soc.*, 2009, **131**, 6050–6051.
7 J.-H. Im, C.-R. Lee, J.-W. Lee, S.-W. Park and N.-G. Park, *Nanoscale*, 2011, **3**, 4088–4093.
8 S. P. Senanayak, B. Yang, T. H. Thomas, N. Giesbrecht, W. Huang, E. Gann, B. Nair, K. Goedel, S. Guha and X. Moya, *Sci. Adv.*, 2017, **3**, e1601935.
9 H.-S. Kim, C.-R. Lee, J.-H. Im, K.-B. Lee, T. Moehl, A. Marchioro, S.-J. Moon, R. Humphry-Baker, J.-H. Yum and J. E. Moser, *Sci. Rep.*, 2012, **2**, 1–7.
10 M. Liu, M. B. Johnston and H. J. Snaith, *Nature*, 2013, **501**, 395–398.
11 Y. Zhou, M. Yang, W. Wu, A. L. Vasiliev, K. Zhu and N. P. Padture, *J. Mater. Chem. A*, 2015, **3**, 8178–8184.
12 N. J. Jeon, J. H. Noh, Y. C. Kim, W. S. Yang, S. Ryu and S. I. Seok, *Nat. Mater.*, 2014, **13**, 897–903.
13 G. E. Eperon, S. D. Stranks, C. Menelaou, M. B. Johnston, L. M. Herz and H. J. Snaith, *Energy Environ. Sci.*, 2014, **7**, 982–988.
14 Y. Zhou, M. Yang, W. Wu, A. L. Vasiliev, K. Zhu and N. P. Padture, *J. Mater. Chem. A*, 2015, **3**, 8178–8184.
15 L. Zuo, Z. Gu, T. Ye, W. Fu, G. Wu, H. Li and H. Chen, *J. Am. Chem. Soc.*, 2015, **137**, 2674–2679.
16 N. K. Noel, S. D. Stranks, A. Abate, C. Wehrenfennig, S. Guarnera, A.-A. Haghighirad, A. Sadhanala, G. E. Eperon, S. K. Pathak and M. B. Johnston, *Energy Environ. Sci.*, 2014, **7**, 3061–3068.
17 K. Wu, X. Zhang, F. Li, D. Xiao, Y. Hou, S. Zhu, D. Liu, X. Ye, M. Ye and J. Yang, *Nat. Commun.*, 2015, **6**, 1–13.
18 C. Huang, W. Fu, C.-Z. Li, Z. Zhang, W. Qiu, M. Shi, P. Heremans, A. K.-Y. Jen and H. Chen, *J. Am. Chem. Soc.*, 2016, **138**, 2528–2531.
19 W. Chen, Y. Wu, Y. Yue, J. Liu, W. Zhang, X. Yang, H. Chen, E. Bi, I. Ashraful and M. Grätzel, *Science*, 2015, **350**, 944–948.
20 S. D. Stranks and H. J. Snaith, *Nat. Nanotechnol.*, 2015, **10**, 391–402.
21 Y. Zhao and K. Zhu, *Chem. Soc. Rev.*, 2016, **45**, 655–689.
22 J.-H. Im, I.-H. Jang, N. Pellet, M. Grätzel and N.-G. Park, *Nat. Nanotechnol.*, 2014, **9**, 927–932.
23 W. Nie, H. Tsai, R. Asadpour, J.-C. Blancon, A. J. Neukirch, G. Gupta, J. J. Crochet, M. Chhowalla, S. Tretiak and M. A. Alam, *Science*, 2015, **347**, 522–525.
24 M. He, D. Zheng, M. Wang, C. Lin and Z. Lin, *J. Mater. Chem. A*, 2014, **2**, 5994–6003.
25 J. S. Yun, A. Ho-Baillie, S. Huang, S. H. Woo, Y. Heo, J. Seidel, F. Huang, Y.-B. Cheng and M. A. Green, *J. Phys. Chem. Lett.*, 2015, **6**, 875–880.
26 V. Gonzalez-Pedro, E. J. Juarez-Perez, W.-S. Arsyad, E. M. Barea, F. Fabregat-Santiago, I. Mora-Sero and J. Bisquert, *Nano Lett.*, 2014, **14**, 888–893.
27 T. Baikie, Y. Fang, J. M. Kadro, M. Schreyer, F. Wei, S. G. Mhaisalkar, M. Graetzel and T. J. White, *J. Mater. Chem. A*, 2013, **1**, 5628–5641.
28 S. Hu, X. Yang, B. Yang, Y. Zhang, H. Li and C. Sheng, *J. Phys. Chem. C*, 2021, **125**, 2212–2219.
29 B. Hailegnaw, S. Kirmayer, E. Edri, G. Hodes and D. Cahen, *J. Phys. Chem. Lett.*, 2015, **6**, 1543–1547.
30 M. Petrović, V. Chellappan and S. Ramakrishna, *J. Sol. Energy*, 2015, **122**, 678–699.
31 D. Bi, P. Gao, R. Scopelliti, E. Oveisi, J. Luo, M. Grätzel, A. Hagfeldt and M. K. Nazeeruddin, *Adv. Mater.*, 2016, **28**, 2910–2915.
32 T. M. Koh, K. Thirumal, H. S. Soo and N. Mathews, *ChemSusChem*, 2016, **9**, 2541–2558.
33 J. Shi, Y. Gao, X. Gao, Y. Zhang, J. Zhang, X. Jing and M. Shao, *Adv. Mater.*, 2019, **31**, 1901673.
34 I. C. Smith, E. T. Hoke, D. Solis-Ibarra, M. D. McGehee and H. I. Karunadasa, *Angew. Chem.*, 2014, **126**, 11414–11417.
35 C. Ma, D. Shen, T. W. Ng, M. F. Lo and C. S. Lee, *Adv. Mater.*, 2018, **30**, 1800710.
36 Y. Zhai, S. Baniya, C. Zhang, J. Li, P. Haney, C.-X. Sheng, E. Ehrenfreund and Z. V. Vardeny, *Sci. Adv.*, 2017, **3**, e1700704.
37 J. Shi, Y. Gao, X. Gao, Y. Zhang, J. Zhang, X. Jing and M. Shao, *Adv. Mater.*, 2019, **31**, 1901673.
38 L. N. Quan, M. Yuan, R. Comin, O. Voznyy, E. M. Beauregard, S. Hoogland, A. Buin, A. R. Kirmani, K. Zhao and A. Amassian, *J. Am. Chem. Soc.*, 2016, **138**, 2649–2655.
39 D. H. Cao, C. C. Stoumpos, O. K. Farha, J. T. Hupp and M. G. Kanatzidis, *J. Am. Chem. Soc.*, 2015, **137**, 7843–7850.
40 T. M. Koh, V. Shanmugam, J. Schlipf, L. Oesinghaus, P. Müller-Buschbaum, N. Ramakrishnan, V. Swamy, N. Mathews, P. P. Boix and S. G. Mhaisalkar, *Adv. Mater.*, 2016, **28**, 3653–3661.
41 H. Tsai, W. Nie, J.-C. Blancon, C. C. Stoumpos, R. Asadpour, B. Harutyunyan, A. J. Neukirch, R. Verduzco, J. J. Crochet and S. Tretiak, *Nature*, 2016, **536**, 312–316.
42 X. Li, M. I. Dar, C. Yi, J. Luo, M. Tschumi, S. M. Zakeeruddin, M. K. Nazeeruddin, H. Han and M. Grätzel, *Nat. Chem.*, 2015, **7**, 703–711.
43 C. Sun, Q. Xue, Z. Hu, Z. Chen, F. Huang, H. L. Yip and Y. Cao, *Small*, 2015, **11**, 3344–3350.
44 C.-C. Chueh, C.-Y. Liao, F. Zuo, S. T. Williams, P.-W. Liang and A. K.-Y. Jen, *J. Mater. Chem. A*, 2015, **3**, 9058–9062.
45 Y. Chen, Y. Zhao and Z. Liang, *J. Mater. Chem. A*, 2015, **3**, 9137–9140.
46 C. Zuo and L. Ding, *Nanoscale*, 2014, **6**, 9935–9938.
47 X. Gong, M. Li, X. B. Shi, H. Ma, Z. K. Wang and L. S. Liao, *Adv. Funct. Mater.*, 2015, **25**, 6671–6678.
48 G. Li, T. Zhang and Y. Zhao, *J. Mater. Chem. A*, 2015, **3**, 19674–19678.
49 S. Yang, W. Liu, L. Zuo, X. Zhang, T. Ye, J. Chen, C.-Z. Li, G. Wu and H. Chen, *J. Mater. Chem. A*, 2016, **4**, 9430–9436.
50 Y. Zhao and K. Zhu, *J. Phys. Chem. C*, 2014, **118**, 9412–9418.
51 W. Ke, C. Xiao, C. Wang, B. Saparov, H. S. Duan, D. Zhao, Z. Xiao, P. Schulz, S. P. Harvey and W. Liao, *Adv. Mater.*, 2016, **28**, 5214–5221.
52 X. Zhang, G. Wu, W. Fu, M. Qin, W. Yang, J. Yan, Z. Zhang, X. Lu and H. Chen, *Adv. Energy Mater.*, 2018, **8**, 1702498.

53 X. Zhang, G. Wu, S. Yang, W. Fu, Z. Zhang, C. Chen, W. Liu, J. Yan, W. Yang and H. Chen, *Small*, 2017, **13**, 1700611.
54 J. Qing, X. K. Liu, M. Li, F. Liu, Z. Yuan, E. Tiukalova, Z. Yan, M. Duchamp, S. Chen and Y. Wang, *Adv. Energy Mater.*, 2018, **8**, 1800185.
55 X. Zhang, X. Ren, B. Liu, R. Munir, X. Zhu, D. Yang, J. Li, Y. Liu, D.-M. Smilgies, R. Li, Z Yang, T. Niu, X. Wang, A. Amassian, K. Zhao and S. Liu, *Energy Environ. Sci.*, 2017, **10**, 2095–2102.
56 J. H. Tsai, I. C. Cheng, C. C. Hsu, C. C. Chueh and J. Z. Chen, *Electrochim. Acta*, 2019, **293**, 1–7.
57 W. Yan, Y. Li, Y. Li, S. Ye, Z. Liu, S. Wang, Z. Bian and C. Huang, *Nano Energy*, 2015, **16**, 428–437.
58 D. H. Kang and N. G. Park, *Adv. Mater.*, 2019, **31**, 1805214.